This is a peer-reviewed, accepted author manuscript of the following article: Mohan, P., Rajak, D. K., Pruncu, C., Behera, A., Amigó-Borrás, V., & Elshalakany, A. B. (Accepted/In press). Influence of β-phase stability in elemental blended Ti-Mo and Ti-Mo-Zr alloys. *Micron*.

Influence of β-phase stability in elemental blended Ti-Mo and Ti-Mo-Zr alloys

Prakash Mohan[1], Dipen Kumar Rajak[2,*], Pruncu I. Catalin[3, 4*], Ajit Behera[5], Vicente Amigó-Borrás[6], Abou Bakr Elshalakany[7,8]

[1,6]Department of Production and Industrial Engineering, Polytechnic University of Valencia, Valencia 46022, Spain

[2]Department of Mechanical Engineering, Sandip Institute of Technology and Research Centre, Nashik 422213, India

[3]Department of Mechanical Engineering, Imperial College London, Exhibition Rd., London SW7 2AZ, UK

[4]Design, Manufacturing & Engineering Management, University of Strathclyde, Glasgow, G1 1XJ, Scotland, UK

[5]Department of Metallurgical & Materials Engineering, National Institute of Technology, Rourkela 769008, India

[7]Production Engineering and Printing Technology Department, Akhbar El Yom Academy, Giza, Egypt

[8]Mechatronics Technology Program, New Cairo Technological University NCTU, 5Th Settlement, Egypt

Corresponding Author: *dipen.pukar@gmail.com, *catalin.pruncu@starth.ac.uk

Abstract

This paper investigated the improvement of mechanical properties for one of the most used biomaterials, titanium-based alloy. To improve its mechanical properties, molybdenum was chosen to be added to Ti and Ti-Zr alloys through a mechanical blending process. After homogenization of Ti (12, 15) Mo and Ti (12, 15) Mo-6Zr, the compaction pressure and sintering temperature were varied to create pellets. Characterization has been done using scanning electron microscopy (SEM), X-ray diffraction (XRD), Vickers's hardness, Archimedes test and ultrasonic method, and 3-point bending test. Micrograph of each pellet revealed the influence of Mo content that plays a prominent role in the variation of microstructure in the alloys Ti-Mo and Ti-Zr-Mo. The porosity and density were also influenced by changing the β-phase. EBSD analysis shows the increase in β-phase with the addition of Zr. The overall results indicated that the percentage of β-phase greatly affects the mechanical properties for the specimens.

Key words: Elemental blend; Mo-Ti, Mo-Ti-Zr, β-phase stability

1. Introduction

In the present era, metallic biomaterials are very helpful for organ implant as they can efficiently replace most of the active body parts such as total knee, hip, locking plates, angle plates, spine, elbow, heal, and dental products [1]. In a competitive way, metallic implants are gradually improving their quality by incorporating various elements in stainless steel and in Ti-based alloys. Stainless steel has also been recorded as the first successful implant material used in the surgical field [1]. Among the wide variety of biomaterials (Co-Cr based alloy, Mo-steel, Ni-Ti based), titanium alloys have proven to be successful implant materials because of their unique characteristics such as excellent bio-compatibility, better mechanical properties (higher toughness, lower Young's modulus, higher strength and hardness), light weight, and excellent corrosion resistance [2-5].

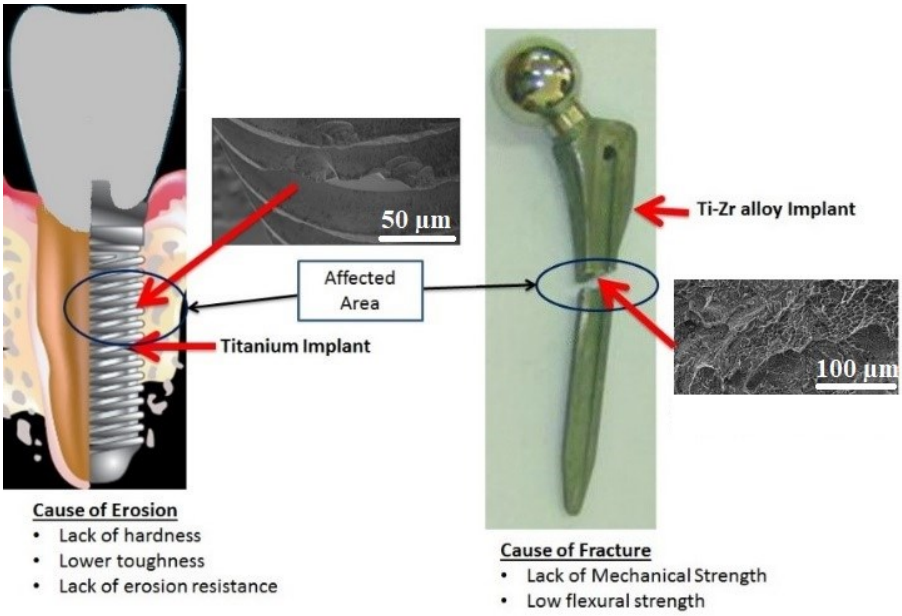

Fig. 1: Defects occurring in Ti-Zr alloys used for dental implant and hip implant

As shown in figure 1, the lack of mechanical strength, hardness, and less toughness in Ti-Zr implant can lead to fracture and erosion. To overcome this problem, adding Mo can be beneficial as Mo improves the mechanical properties and improves corrosion resistance. There are three main categories of titanium alloys based on different phases: α-phase Ti, (α+β)-phase, and β-phase. Pure Ti is the α-phase category. Ti-6Al-4V and Ti-6Al-7Nb are (α+β) phase alloys, whereas β-alloys include Ti-15Mo, Ti-15Mo-3Nb, Ti-12Mo-6Zr-2Fe [2], Ti-15Zr-4Nb-4Ta-0.2Pd, Ti-15Mo-5Zr-3Al, Ti-35.3Nb-5.1Ta-7.1Zr and Ti-29Nb-13Ta-4.6Zr. Moreover, α-phase, β-phase, and (α+β)-phase have different modulus. For metallic biomaterial, higher strength with lower modulus is relevant. Bone modulus should be in the range of 4-30 GPa, basing on bone alignment and axis of measurement. At present, some implant materials with considerable strength have greater stiffness than the replaced material (bone), indicating the easy transfer of the generated stress to the connected bone which results cell damage and implant loosening, considered as biomechanical incompatibility. This is known as stress shield effect. Hence, the material to be chosen in implant have higher strength and lower modulus to shut off the implant failure and ensure higher working period and keeping away from revision surgery [4]. Therefore, β-phase stabilized metallic material should be adopted. Elements that depress the transformation temperature, readily dissolve in, strengthen the β-phase, and exhibit low α-phase solubility are known as β-stabilisers. Mo is the β-isomorphous element exhibiting complete mutual solubility, which can increase the coherency in Ti-alloy to improve the mechanical strength.

Ti-alloys are in demand as they have lower modulus (55-110 GPa) compared to 316L SS (~210 GPa) and Cr-Co alloys (~240 GPa). Along with the low modulus of titanium, some of the properties such as higher tensile strength (220MPa), lower density (4.50 g/cm^3), high resistance to corrosion, greater inertness with living cell, greater biocompatibility, and high specific strength makes Ti the most suitable implant [5]. Several studies have examined β- phase Ti-alloy [6]. Some elements such as V and Al can give β-phase stability as well as toxic effect. Avoiding this bio incompatibility, it is suitable to add Mo and Zr for β-phase. Studies on Ti-Mo alloy and Ti-Mo-Zr based alloys by a list of researchers are discussed in the following paragraphs.

Zhang et al. (2015) studied on Ti-xMo (x=6.20-21.5 wt.%) composition using arc-melting process (non-consumable) and casting process to analyse the elastic modulus of phases present in Ti-Mo alloys. He found the sensitiveness of phase formation in presence of Mo percentage and Ti-8Mo alloy has 82.98 GPa elastic modulus [7]. Martins et al. (2011) studied on Ti-15Mo prepared by Arc-melting furnace to synthesis the Ti15Mo alloy for considering in biomaterial application. He found by adding Mo up to 15%, there was gradual increase in density and microhardness, while reduction in the elastic modulus with respect to CP-Ti and β-type Ti alloys [8]. Chen et. al. (2006) fabricated Ti-xMo (x=5-20) by casting process to study their microstructure and properties. They found that, when Mo is more than 15%, only equixed β-crystal grains are formed, hardness, compression strength and elastic modulus found out 451 HV and 1636 MPa and 29.8 GPa respectively [9]. Nishimura (2011) prepared 3Mo5FeTi alloy by arc melting to evaluate the corrosion resistance. Here the Fe content is not responsible to decreases the corrosion resistance of the aged Mo-Fe-Ti alloy. α-phase precipitation in aged alloy results lower corrosion resistance than that of no α-phase content but have much higher resistance than pure Ti [10]. Similarly, several researchers found out the higher strength, modulus, corrosion resistance and biocompatibility by incorporating the Mo in Ti-alloys [11-24]. Again, the addition of Zr enabled the enhancement of β phase stabilization [16-24]. Zr is in the same chemical group as Ti and can improve the mechanical strength as well as biocompatibility when incorporated in Ti-alloys [17]. Also, Mo act as a strong β-stabilizer that can reduce the young's modulus and increase the corrosion resistance in Ti-alloys [8]. Incorporation of both the element in Ti-alloys has been studied by several researcher in literature. This paper focused on increasing the β-phase in titanium by varying the additive elements of Mo and Zr. The Mo and Zr percentages are varied in the alloy to generate better physical properties and mechanical properties.

2. Material and methods

2.1 Preparation of powders

Titanium and molybdenum with 99.7% and 99.95% purity and particle sizes 44 μm and 8 μm, respectively, were procured from Atlantic Equipment Engineers (AEE). Further, zirconium with purity 99.95% and 44 μm was purchased from Alfa Aesar. For homogenization, an elemental blend of Ti (12, 15%) Mo and Ti (12,15%) Mo-6Zr was created using tubular mixer equipment for 30 minutes at 150 RPM.

2.2 Processing of pellet

The homogenized elemental blend powder was compacted using the universal testing machine (Instron 432 Model) with 500 kN compressive load and 600 MPa compaction pressure to produce 32x12x6 mm^3 dimensional specimen. Approximately 8 g powder by weight was required to compact the above dimension using uniaxial hydraulic press. The compacted specimen sintered in a high vacuum tubular furnace (Carbolite HVT 15/75/450) at temperature 1250 °C with dwell time 3 h and cooled at 10 °C/min.

2.3 Characterization of the sintered samples

Surface morphology analysis of each sintered sample was conducted using optical microscopy (Nikon LT100) and using scanning electron microscopy (Jeol JSM 6300) at different magnifications. The image analysis software employed for quantifying α-phase, β-phases and internal porosity. Microstructure has been studied using both backscattered electron mode and secondary electron mode at different magnifications in SEM.

Further, elemental analysis was performed by energy dispersive spectroscopy (EDS). Phase analysis was measured using X-Ray diffractrometer (Bruker D2 phaser). The microhardness of polished alloys was measured using a microhardness tester (Matsuzawa MXT70) at a load of 200 g for 15 s. An ultrasonic test was also conducted using Karl Deutsch digital Echo graph to measure elastic modulus. For surface morphology analysis and phase identification, specimen surface was treated with SiC sand paper polishing followed by very fine disc polishing with a 1 µm rough disc. Three-point bending analysis has done using desktop mechanical tester (Shimadzu AGS-500D, Tokyo, Japan), calculated according to ASTM D-790M, as shown in **supplementary Figure S1**. A three-point bending test can help to determine the bending strength, elongation, and bending strain. Here, L= 22 mm and D= 10 mm (diameter of the supporting wheel). Overall porosity was measured using the Archimedes test. Fractography of the breaking sample was observed through the SEM to analyse the fragility or ductility of the sample. It should be noted that higher percentage of Mo increases the porosity whereas adding ZrH_2 reduces the porosity, and similarly happened in case of sintered density.

3. Result and Discussions

The shape of the Ti powder is angular as depicted in figure 2a with a size range 10-100 µm as confirmed in figure 2d. The shape of the Mo powder is spherical (figure 2b) with 1-10 µm particle size (figure 3e) and Zr powder is a both spherical/angular shape (figure 2c) with size range of 2-38 µm (figure 2f). The figure clearly indicates the presence of Mo at inter-granular space, during green sintering. The morphology of these three powders shows that different shapes and size of the particles reduces the intergranular spacing which leads to a dense structure and compact after sintering.

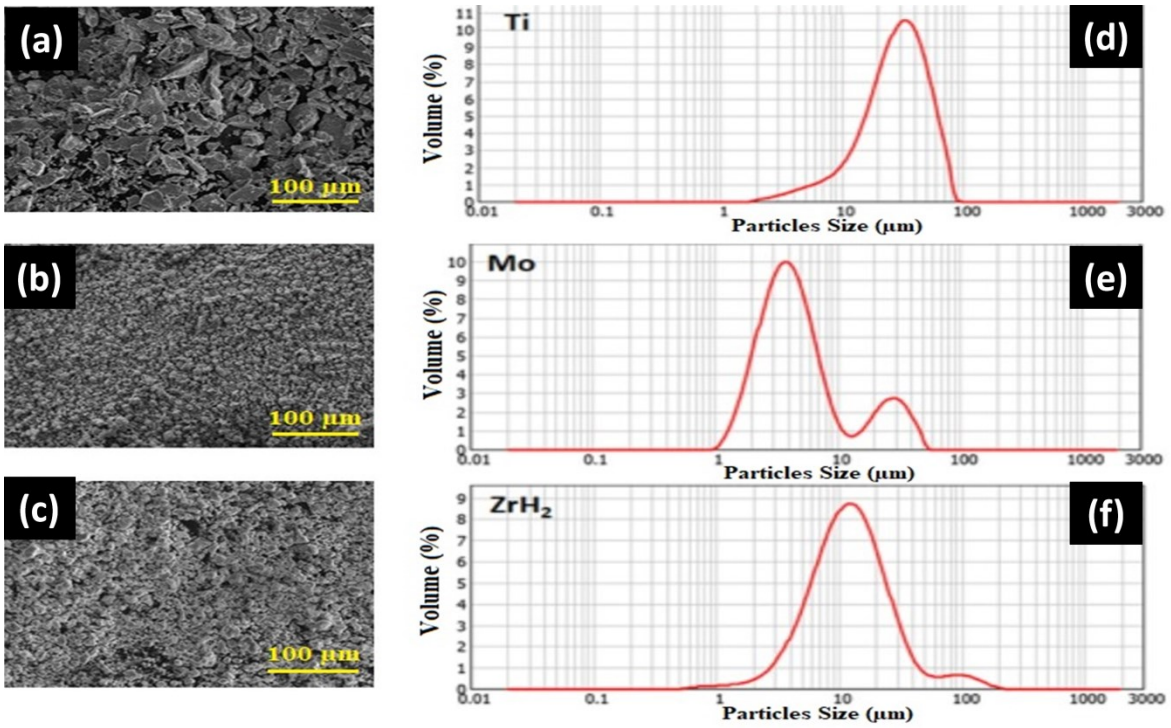

Fig 2: Surface morphology of (a) Ti, (b) Mo, and (c) Zr and their granulometry given in (d), (e), and (f) respectively

3.2 Morphology of pellet

Supplementary figure S2 (a) and (b) shows the surface morphology of Ti12Mo and Ti15Mo. Ti12Mo has bigger grain size than Ti15Mo. Moreover, there is higher β-phase in Ti15Mo compared to that in Ti12Mo. Presence of β-phase is confirmed by the EDS analysis and it is found that β-phase increases by increasing the percentage of Mo. Hence, it can be said that Mo is a strong β stabilizer. Moreover, pores are presented inside the alloy which has an approximately circular shape and is denoted by the arrow mark in the **supplementary figure S2**. Further, α-phase is mainly on the grain boundary of the sintered samples, and to an extent, inside the alloy. **Supplementary figure S3** show the surface morphology of Ti-12Mo-6Zr and Ti-15Mo-6Zr. It is found that the grain size of Ti-12Mo-6Zr is greater than that of Ti-15Mo-6Zr. β-phase percentage is also higher in Ti-15Mo-6Zr as comparison with Ti-12Mo-6Zr, which is confirmed by EDS as well as from XRD analysis which shows that Mo enhanced the percentage of β. Further, pores are present mostly inside the grain which have a relative circular shape. In addition, α-phase is distributed mainly on the grain boundary of the sintered samples, with also some evidence were found inside the alloy. However, β-phase primarily lies inside the alloy. This is true for Ti-12Mo-6Zr as well as Ti-15Mo-6Zr. Ti-15Mo-6Zr also has the highest β-phase available among all the alloys, as confirmed by the XRD analysis.

Figure 3(a-d) shows XRD pattern of Ti-12Mo, Ti-15Mo, Ti-12Mo-6Zr, and Ti-15Mo-6Zr, and the percentage of various phases are given in table 1. The crystal is significantly affected by an increase in Mo % from (12 to 15). Although, Ti-12Mo has less β% (46.3) than Ti-15Mo (49.39%), both are α+β type alloys with α % higher than β in both cases. Adding Zr also improves the percentage of β as seen in Ti-12M-6Zr. Here, the β-phase was found about 59.97%, which is much more than that of α-phase of 46.3%. So, it is found that, Zr shows its β-stabilizing character along with Mo. In case of Ti-15Mo-6Zr, β-phase is dominating which is confirmed by the X-Ray analysis. Table 1 shows that the percentage of β is maximum in case of Ti15Mo6Zr at 83.74% and minimum for Ti12Mo at 46.3%.

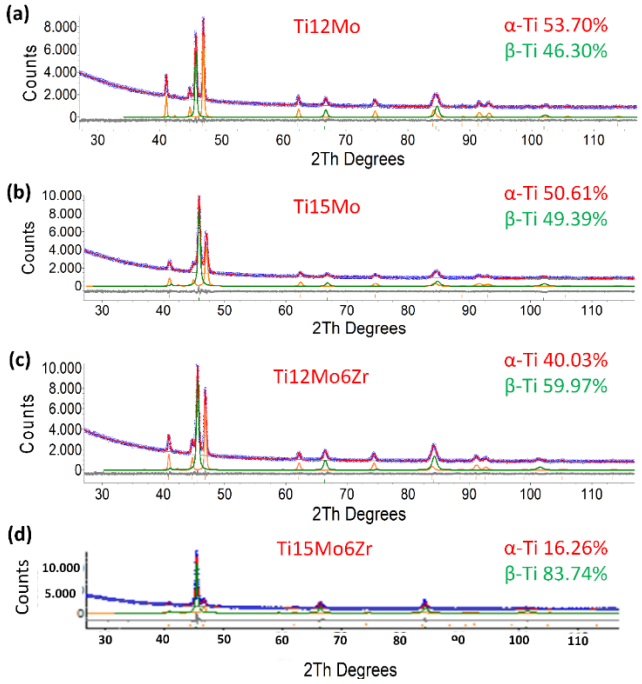

Fig. 3: XRD patterns for the sintering (a) Ti-12Mo, (b) Ti-15Mo, (c) Ti-12Mo-6Zr, and (d) Ti15Mo6Zr

Table 1: Percentage of various phases

Alloy	α-phase (%)	β-phase (%)
Ti-12Mo	53.7	46.3
Ti-12Mo-6Zr	40.03	59.97
Ti-15Mo	50.61	49.39
Ti-15Mo-6Zr	16.26	83.74

Supplementary figure S4, shows the porosity of the sintered samples. Porosity increases by taking more percentage of Mo. It is found that Ti-15Mo have more porosity of 3.12 % than Ti-12Mo (2.93%), which was also observed in Ti-15Mo-6Zr. Ti-15Mo-6Zr (2.71 %) also had higher porosity than Ti-12Mo-6Zr (2.03 %). It was noted that by adding Zr decreased the percentage of porosity. Moreover, Ti12Mo6Zr showed less porosity than Ti-12Mo, while Ti-15Mo-6Zr showed less porosity than Ti-15Mo. It is clear for the slop of the plot from **supplementary figure S4**; with the presence of Mo, the porosity increases by increase in Ti percentage. **Supplementary figure S5** that was generated using the calculation of the equation 1 gives the value of percentage of density when was varied the Molybdenum addition.

$$\Delta D = \frac{Sintered\ density - Green\ density}{Green\ density} \times 100 \quad (1)$$

The ΔD for Ti-12Mo-6Zr is the highest among all the alloys at approximately 26.5%. Further, the value of sintered density 26.5% is higher than green density and the value for Ti15Mo is the least among all at approximately 24%. Further, sintered density is the highest for Ti-12Mo-6Zr (97.97%) and lowest for Ti-15Mo (96.88%). Green density is the highest for Ti-15Mo (78.11%) and lowest for Ti-15Mo-6Zr (77.64%). Because of the highest green density and lowest sintered density of Ti-15Mo, the density difference is kept at a minimum. Generally, the hardness should have a higher value for biomaterial implant material. Supp**lementary figure S6** shows that adding a higher percentage of Mo increases the value of hardness. The range of hardness measured was between 283 and 322 Hv. When the % of Mo changes from 12 to 15, the hardness increases by approximately 9% from 283 to 309. Adding Zr also improves hardness for Ti-12Mo (283 Hv) to Ti-12Mo-6Zr (308 Hv) by approximately 8.7% and from Ti-15Mo (309 Hv) to Ti-15Mo-6Zr (322 Hv) by approximately 4.2%. Ti-15Mo also has more hardness than Ti-12Mo. Moreover, adding Zr improves the hardness values as it can be observed that Ti-12Mo-6Zr has a higher hardness value than Ti-12Mo while Ti-15Mo-6Zr has a slightly higher hardness value than Ti-15Mo. Ti-15Mo-6Zr also has the highest value (approx. 322 HV) among all alloys, which makes this alloy more promising for biomaterials use. **Supplementary figure S7** shows the elastic modulus (GPa) with different % of Mo for Ti-Mo and Ti-6Zr-Mo. Elastic modulus forms the main property for biomaterial implant; the value should be less and should be near the bone modulus. Hence, β-Ti alloy are a better implant material as they have less elastic modulus. From figure 10; the presence of Mo reduces the elastic modulus in both the system Ti-Mo & Ti-Mo-Zr system also. When the percentage of Mo for Ti-Mo increases from 12% to 15%, the elastic modulus decreases slightly from 104.09 to 103.84 GPa, as it also does for Ti-6Zr-Mo with the value of elastic modulus decreasing from 102.90 Gpa to 98.55 GPa for Ti12Mo6Zr and Ti15Mo6Zr, respectively. Elastic modulus is the highest for Ti12Mo at approximately 104.2 GPa. Adding Zr with Ti-Mo alloy also reduces the value of elastic modulus. Thus, considering all alloy combinations,

Ti15Mo6Zr can be regarded as the best alloy with the least elastic modulus and has a value of approximately 98.5 GPa.

Supplementary figure S8, shows the bending strength and their fractography with different % of Mo for Ti-Mo and Ti-6Zr-Mo. When the percentage of Mo changes from 12% to 15%, the bending strength increases in Ti-15Mo while it decreases in Ti-15Mo-6Zr. The decrease of bending strength in Ti-15Mo-6Zr occurs because of the presence of Zr in this alloy. In case of Ti-15Mo, the bending strength increases because of the higher percentage of % of Mo. Ti-l5Mo has the maximum value of bending strength at approximately 2161 MPa and Ti-15Mo-6Zr has the lease value at approximately 1650 MPa. Adding Zr decreases the value of bending strength. Hence, the bending strength of Ti-12Mo-6Zr and Ti-15Mo-6Zr is less than Ti-12Mo and Ti-15Mo, respectively. From the fractography image of all alloys, it is evident that it is a mixed fracture (brittle+ductile) but requires the maximum energy in case of Ti-15Mo. Table 2 presents the flexural strength (energy required for breaking the sintered samples) of all the specimen, in which 50.37± 10.36 J, 48.52± 2.37 J, 36.59± 5.03 J and 26.07± 4.48 J is found out in Ti-12Mo, Ti-15Mo, Ti-12Mo-6Zr, and Ti-15Mo-6Zr respectively. The minimum energy is found out in Ti-15Mo-6Zr and maximum for Ti-12Mo.

Table 2: Energy and deformation calculated by Flexural test for Ti-Mo base alloy

Alloys	Deformation (%)	Energy(J)
Ti-12Mo	0.05	50.37± 10.36
Ti-15Mo	0.05	48.52± 2.37
Ti-12Mo-6Zr	0.04	36.59± 5.03
Ti-15Mo-6Zr	0.03	26.07± 4.48

Figure 4 shows the EBSD images of Ti-12Mo and Ti-12Mo-6Zr which includes Euler colours, IPF X, and phases of the after-sinter. The grains are equiaxed and the grain size vary. Some big grains are found near the small grains. The blue lines in the phase's image indicate the percentage of α inside the alloy. It is thus evident that, in case of Ti-12Mo, higher percentage of α is available than for Ti-12Mo-6Zr. This means that, in this case, Zr functions like a β-stabilizer which is also confirmed by the XRD image of Ti-12Mo-6Zr shown in **supplementary figure S3**. With the help of AzTec software, the grain size of Ti-12Mo and Ti-12Mo-6Zr were calculated for the present study. It was observed that the grain size for Ti-12Mo was 6.89 μm, with α grain size at 4.97 μm and β grain size at 8.59 μm. Moreover, the overall grain size for Ti-12Mo-6Zr was 6.85 μm, with α grain size at 6.21 μm and β grain size at 7.47 μm. Thus, in case of both alloys, for β-grain had a larger size than α- grain. In case of Ti-12Mo-6Zr, β grain size dominates that of Ti-12Mo.Further, the percentage of α and β were also calculated for Ti12Mo and Ti-12Mo-6Zr using phases diagram, as shown in figure 4 (c) for Ti-12Mo and 4(f) for Ti-12Mo-6Zr. It was noted that, for Ti-12Mo, α and β were at 41.3% and 58.7%, respectively, and for Ti-12Mo-6Zr, α and β were at 27.7% and 72.3%, respectively. Hence, the EBSD analysis shows that by adding Zr, grain size reduces with increase in the percentage of β.

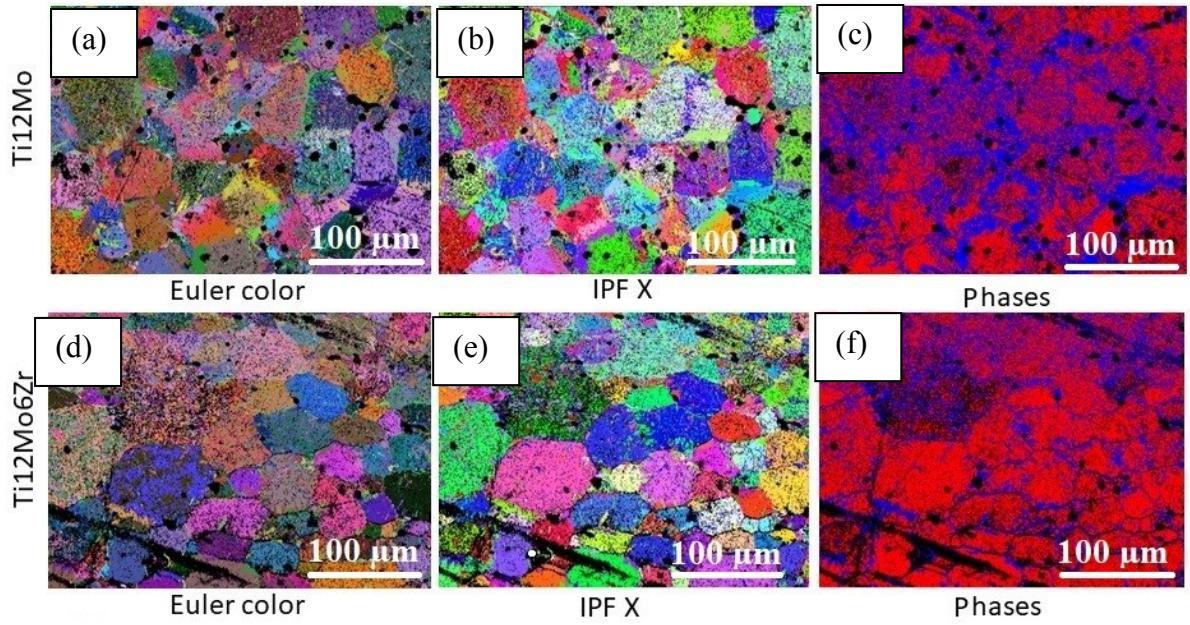

Fig. 4: (a) Euler colour image of Ti12Mo, (b) IPF X image of Ti12Mo, (c) Colour plot of various phases of Ti12Mo, (d) Euler colour image of Ti12Mo6Zr, (e) IPF X image of Ti12Mo6Zr, (f) Colour plot of various phases of Ti12Mo6Zr

4. Conclusions

This work shows that Mo improves β-stability when the percentage of Mo increases from 12% to 15 %. Porosity was observed to be much less in all alloys at approximately 3% in all cases. Moreover, Ti (12,15) Mo6Zr showed greater β-phase in terms of Ti-12Mo and Ti-15Mo. Beta - phase was also the highest for Ti-15Mo-6Zr, as confirmed by an XRD analysis, SEM, and EBSD. It was further noted that the elastic modulus was less in all alloys associated to Ti-6Al-4V and Ti G4, while Ti-15Mo-6Zr had the least elastic modulus, thus confirming that the higher β-phase is the main reason for less elastic modulus. Moreover, smaller elastic modulus is best suited for a biomaterial implant, as discussed by different authors. Further, bending modulus was the highest in Ti-15Mo, indicating the strengthening effect of Mo, and hardness was the maximum in Ti-15Mo-6Zr because of the strengthening effect of Zr and Mo. The EBSD analysis clearly shows that β-grain size is bigger in Ti-12Mo-6Zr compared to Ti-12 Mo, thus confirming the β-stabilizing effect of Zr in addition to the β-stabilizer element. The microstructural analysis also shows that Mo as well as Zr improve the β-phase.

Conflict of interest

On behalf of all authors, the corresponding author states that there is no conflict of interest.

Supplementary data

Figure's

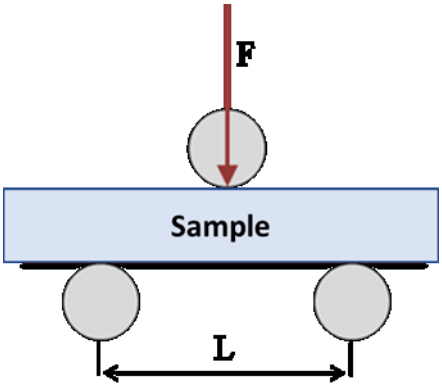

Figure S1: Schematics of 3-point bend test, where L is the distance between supports and the applied force F, L is the length of the sample

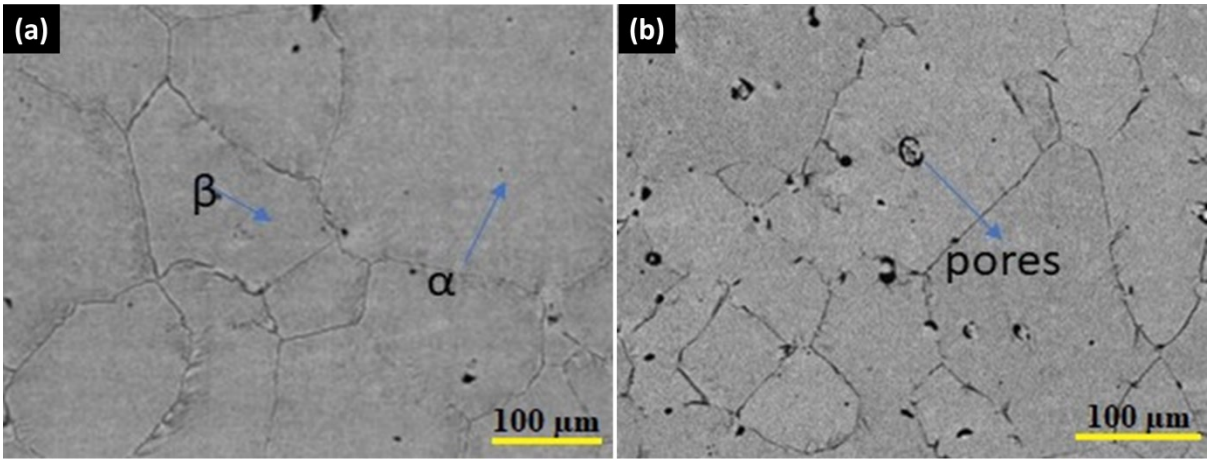

Figure S2: Microstructure of sintered Ti-Mo base alloy at magnification 500X (a) Ti-12Mo (b) Ti-15Mo

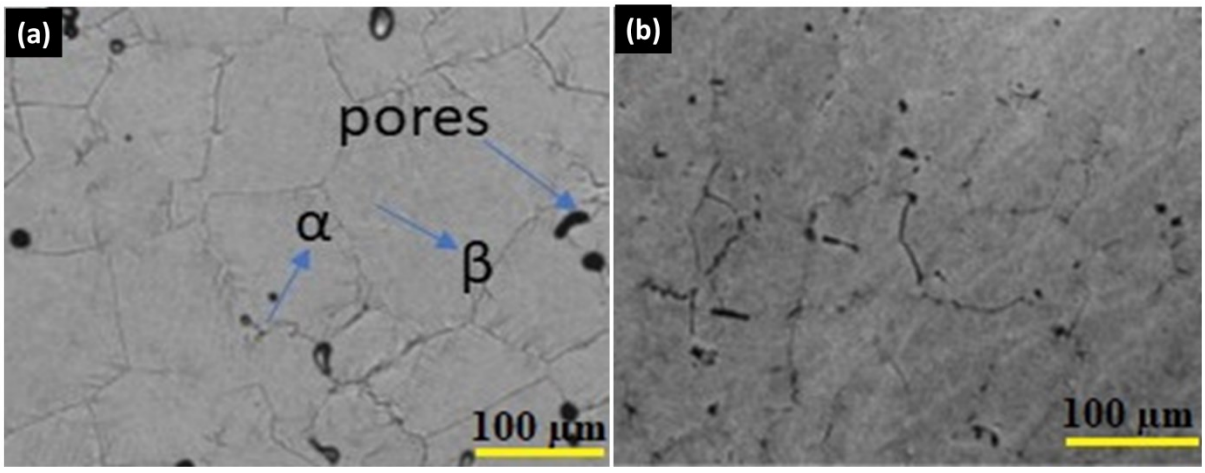

Figure S3: Microstructure of sintered Ti-Mo base alloy at magnification 500X (a) Ti-12Mo-6Zr (b) Ti-15Mo-6Zr

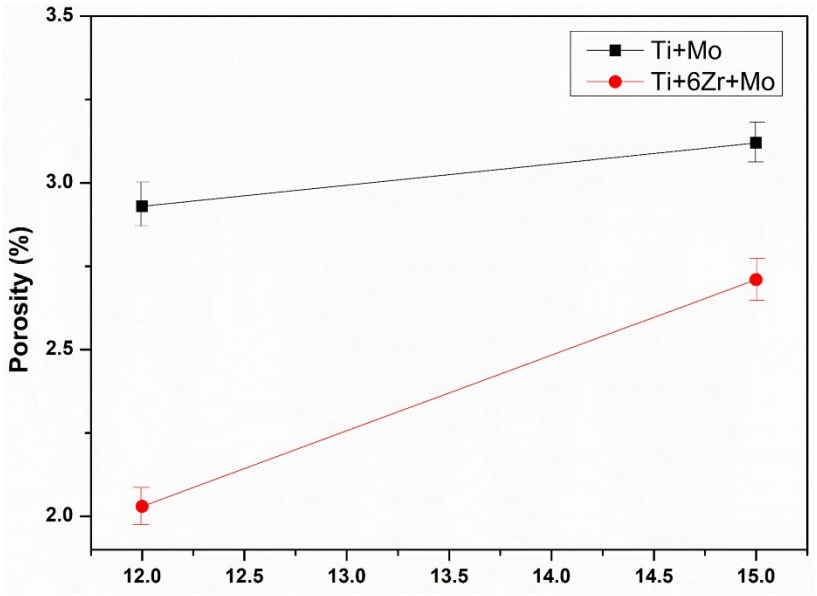

Figure S4: Measurement of porosity with increase in the weight percentage of Mo (sample prepared at 1250 °C)

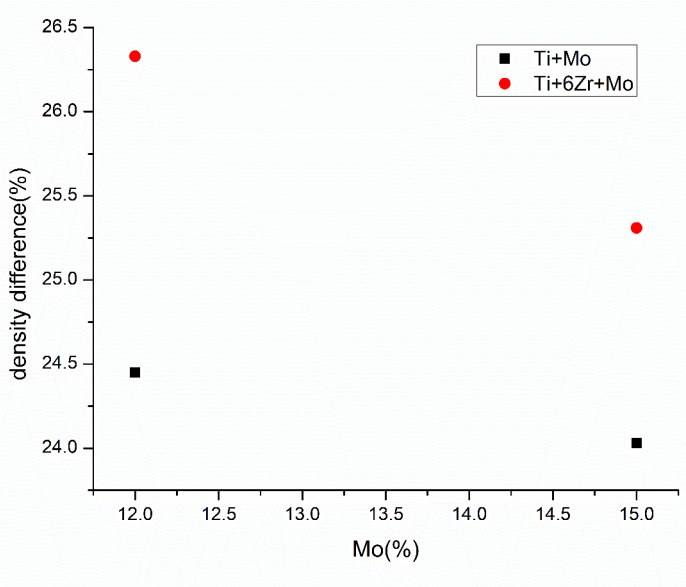

Figure S5: Density difference with respect to the increase in weight percentage of Mo

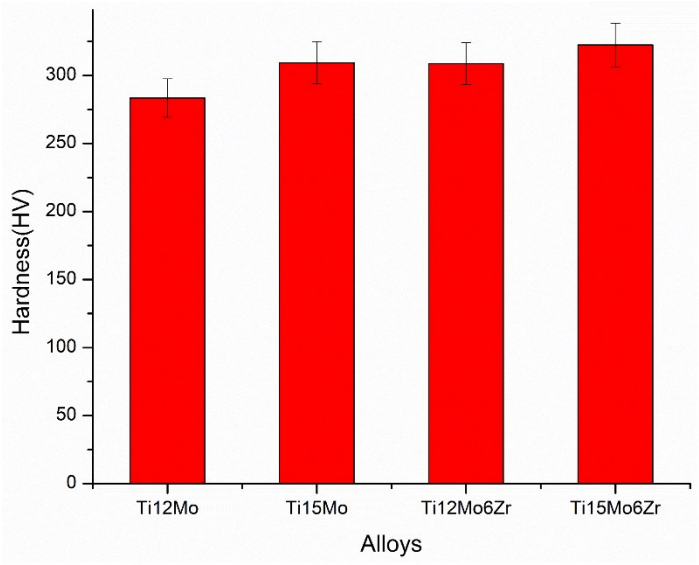

Figure S6: Vickers's Hardness value of Ti12Mo, Ti15Mo, Ti12Mo6Zr, and Ti15Mo6Zr alloy

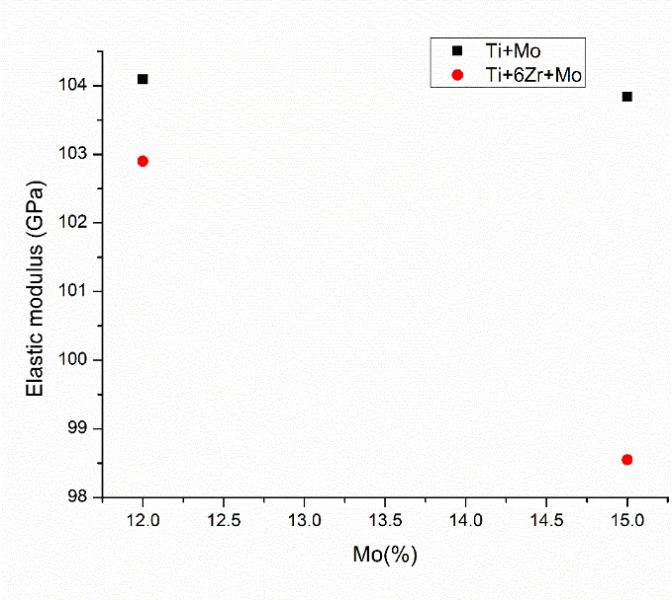

Figure S7: Elastic modulus (GPa) with increasing the Mo weight percentage in Ti-Mo and Ti-6Zr-Mo alloys

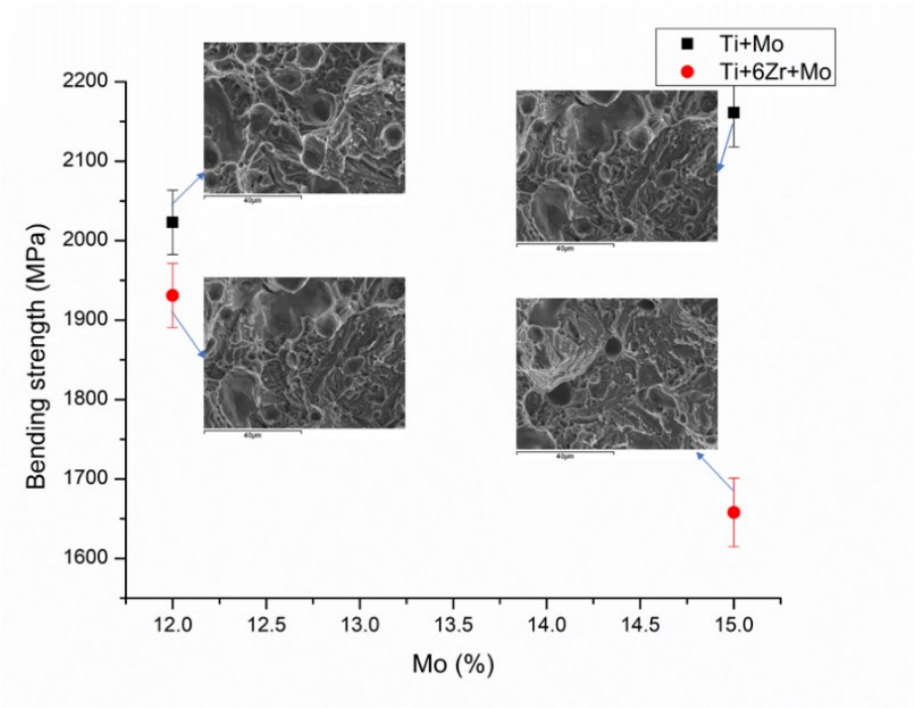

Figure S8: Bending strength (MPa) and their fractography with increasing the Mo weight percentage in Ti-Mo and Ti-6Zr-Mo alloys

References

[1] G. Im, "Biomaterials in orthopaedics: the past and future with immune modulation", Biomater Res, vol 24, pp. 1-4, 2020.

[2] V.D. Cojocaru, A. Nocivin, C. Trisca-Rusu, A. Dan, R. Irimescu, D. Raducanu, B. M. Galbinasu, Improving the Mechanical Properties of a β-type Ti-Nb-Zr-Fe-O Alloy, Metals, vol. 10, pp. 1491, 2020.

[3] A. Behera, P. Mallick, S. S. Mohapatra, "Nanocoatings for anti-corrosion: Materials, Fabrications and Applications", Corrosion Protection at the Nanoscale, Elsevier publisher, ISBN no: 978-0-12-819359-4, pp. 449-457, 2020.

[4] S. Gürgen, S. F. Diltemiz, M. C. Kuşhan, "Oxidation and thermal shock behavior of thermal barrier coated 18/10CrNi alloy with coating modifications", J Mech Sci Technol, vol. 31, pp. 149-155, 2017.

[5] C. Prakash, S. Singh, C. I. Pruncu, V. Mishra, G. Krolczyk, D. Y. Pimenov, A. Pramanik, "Surface Modification of Ti-6Al-4V Alloy by Electrical Discharge Coating Process Using Partially Sintered Ti-Nb Electrode", Materials, vol. 12, pp. 1-16, 2019.

[6] E. U. Solakoğlu, S. Gürge, M. C. Kuşhan, "Surface topography of nickel based superalloy manufactured with direct metal laser sintering (DMLS) method", Surface Topography: Metrology and Properties, vol. 7, pp. 1-12, 2019.

[7] W. D. Zhang et al., “Elastic modulus of phases in Ti-Mo alloys,” Mater. Charact., vol. 106, pp. 302–307, 2015.

[8] J. R. S. Martins Júnior et al., “Preparation and characterization of Ti-15Mo alloy used as biomaterial,”

Mater. Res., vol. 14, no. 1, pp. 107-112, 2011.

[9] Y. Y. Chen, L. J. Xu, Z. G. Liu, F. T. Kong, and Z. Y. Chen, “Microstructures and properties of titanium alloys Ti-Mo for dental use,” Trans. Nonferrous Met. Soc. China (English Ed., vol. 16, no. SUPPL., pp. 2–6, 2006.

[10] T. Nishimura, “Corrosion resistance of Mo-Fe-Ti alloy for overpack in simulating underground environment,” Nucl. Eng. Des., vol. 241, no. 12, pp. 4745-4749, 2011.

[11] C. Pang et al., “β Zr-Nb-Ti-Mo-Sn alloys with low Young’s modulus and low magnetic susceptibility optimized via a cluster-plus-glue-atom model,” Mater. Sci. Eng. A, vol. 626, pp. 369-374, 2015.

[12] D. M. Gordin, I. Thibon, A. Guillou, M. Cornen, and T. Gloriant, “Microstructural characterization of nitrided beta Ti-Mo alloys at 1400 °C,” Mater. Charact., vol. 61, no. 3, pp. 376-380, 2010.

[13] Y. Bao et al., “High strength, low modulus and biocompatible porous Ti-Mo-Fe alloys,” J. Porous Mater., vol. 21, no. 6, pp. 913–919, 2014.

[14] L. D. Zardiackas, D. W. Mitchell, and J. a. Disegi, “Characterization of Ti-15Mo beta titanium alloy [orthopedic implants],” Proc. 1997 16 South. Biomed. Eng. Conf., pp. 95-98, 1997.

[15] N. T. C. Oliveira, G. Aleixo, R. Caram, and A. C. Guastaldi, “Development of Ti-Mo alloys for biomedical applications: Microstructure and electrochemical characterization,” Mater. Sci. Eng. A, vol. 452–453, pp. 727-731, 2007.

[16] D. R. N. Correa et al., “Development of Ti-15Zr-Mo alloys for applying as implantable biomedical devices,” J. Alloys Compd., vol. 749, pp. 163-171, 2018.

[17] W. F. Ho, S. C. Wu, S. K. Hsu, Y. C. Li, and H. C. Hsu, “Effects of molybdenum content on the structure and mechanical properties of as-cast Ti-10Zr-based alloys for biomedical applications,” Mater. Sci. Eng. C, vol. 32, no. 3, pp. 517-522, 2012.

[18] A. Behera, S. S. Mohapatra, D. K. Verma, "Nanomaterial: Fundamental Principle and Application", Nanotechnology and Nanomaterial applications in food, health and biomedical science, Apple Academic Press & CRC press, ISBN: 9781771887649, 343 pg, 2019.

[19] M. F. Ijaz, H. Y. Kim, H. Hosoda, and S. Miyazaki, “Superelastic properties of biomedical (Ti-Zr)-Mo-Sn alloys,” Mater. Sci. Eng. C, vol. 48, pp. 11-20, 2015.

[20] N. Nomura et al., “Mechanical properties of porous Ti-15Mo-5Zr-3Al compacts prepared by powder sintering,” Mater. Sci. Eng. C, vol. 25, no. 3, pp. 330-335, 2005.

[21] D. R. N. Correa et al., “Effect of the substitutional elements on the microstructure of the Ti-15Mo-Zr and Ti-15Zr-Mo systems alloys,” J. Mater. Res. Technol., vol. 4, no. 2, pp. 180-185, 2015.

[22] X. Zhao, M. Niinomi, and M. Nakai, “Relationship between various deformation-induced products and mechanical properties in metastable Ti-30Zr-Mo alloys for biomedical applications,” J. Mech. Behav. Biomed. Mater., vol. 4, no. 8, pp. 2009-2016, 2011.

[23] R. Banerjee, S. Nag, J. Stechschulte, and H. L. Fraser, “Strengthening mechanisms in Ti-Nb-Zr-Ta and Ti-Mo-Zr-Fe orthopaedic alloys,” Biomaterials, vol. 25, no. 17, pp. 3413-3419, 2004.

[24] S. Nag, R. Banerjee, and H. L. Fraser, “Microstructural evolution and strengthening mechanisms in Ti-Nb-Zr-Ta, Ti-Mo-Zr-Fe and Ti-15Mo biocompatible alloys,” Mater. Sci. Eng. C, vol. 25, no. 3, pp. 357-362, 2005.